Geophys. J. Int. (2012) **191,** 517–529 doi: 10.1111/j.1365-246X.2012.05627.x

Is there a normal magnetic-polarity event during the Palaeocene–Eocene thermal maximum (∼55 Ma)? Insights from the palaeomagnetic record of the Belluno Basin (Italy)

Edoardo Dallanave,[1,2]* Giovanni Muttoni,[2,3] Claudia Agnini,[1] Lisa Tauxe[4] and Domenico Rio[1]

[1]*Department of Geosciences, University of Padova, Via G. Gradenigo* 6, I-35131, *Padova, Italy. E-mail: dallanave@geophysik.uni-muenchen.de*
[2]*Alpine Laboratory of Paleomagnetism (ALP), Via Madonna dei Boschi* 76, I-12016, *Peveragno (CN), Italy*
[3]*Department of Earth Science, Via Mangiagalli* 34, I-20133, *Milano, Italy*
[4]*Scripps Institution of Oceanography, UCSD,* 9500 *Gilman Drive, La Jolla,* CA 92093-0220, *USA*

Accepted 2012 July 24. Received 2012 June 18; in original form 2012 February 25

SUMMARY

In the lowermost Eocene sedimentary record of Ocean Drilling Program Site 1262 (Leg 208, Walvis Ridge, South Atlantic Ocean), the presence of a ∼53-kyr-long normal polarity event has been recorded within the ∼2.55-Myr-long reverse polarity Chron C24r (∼53.3–55.9 Ma) and termed Palaeocene–Eocene magnetic reversal (PEMR). The origin of the PEMR has been speculatively related to a change in the Earth's rotation rate that was in turn influenced by an abrupt overturning of the ocean-atmosphere circulation that occurred during the Palaeocene–Eocene thermal maximum (PETM) at ∼55 Ma. Such provocative genesis for a magnetic-polarity reversal demands the PEMR to be confirmed (or refuted) in additional PETM sections. Here, we present detailed palaeomagnetic and rock-magnetic data from the Forada and Cicogna sections of the Belluno Basin in NE Italy, which contain an expanded and continuous record of the PETM termed clay marl unit (CMU). Our data indicate that these sediments were deposited during a continuous interval of reverse geomagnetic field polarity. We therefore conclude that no magnetic-polarity reversals occurred throughout the PETM. In addition, we studied the origin of the high degree of flattening affecting the characteristic magnetic component directions of the sediments, which we interpret as due to a combination of depositional inclination shallowing typical of detrital haematite, and post-depositional compaction of clays, particularly abundant in the carbonate-depleted CMU.

Key words: Magnetostratigraphy; Reversals: process, timescale, magnetostratigraphy; Rock and mineral magnetism.

1 INTRODUCTION

The Earth's magnetic field during the ∼2.55-Myr-long Chron C24r is characterized by the presence of a series of 11 cryptochrons (Cande & Kent 1992a,b, 1995), which could represent either intervals of low palaeointensity or short-lived polarity chrons. Recently, Lee & Kodama (2009) reported the occurrence of a normal polarity event within Chron C24r at Ocean Drilling Program (ODP) Site 1262 (Leg 208, Walvis Ridge, South Atlantic Ocean). This event, referred to as PEMR (Palaeocene-Eocene magnetic reversal), was found in calcareous nannoplankton zone NP10 (see Agnini *et al.* 2007a) embedded in the so-called Clay Layer, which is the lithological expression of the Palaeocene–Eocene thermal maximum (PETM; e.g. Zachos *et al.* 2001, 2005) at Walvis Ridge sites (see Zachos *et al.* 2004 for a description of the PETM at ODP Site 1262). Lee & Kodama (2009) interpreted the PEMR as a global event after correlation with the N1(?) normal polarity event described by Tauxe *et al.* (1994) in the Willwood Formation of the southern Bighorn Basin (Wyoming) as well as with similar short-lived normal polarity events in Deep Sea Drilling Project (DSDP) Site 550 (Leg 80, Goban Spur, NE Atlantic; Townsend 1985) and ODP Site 690 (Leg 113, Weddell Sea, Southern Ocean; Spiess 1990). Lee & Kodama (2009) suggested that a possible abrupt overturning in the global ocean circulation during the PETM (Nunes & Norris 2006), accompanied with a change of the atmospheric patterns, may have driven the PEMR by changing the interaction between the Earth's mantle and the outer core and influencing the Earth's rotation rate.

However, reasonable doubts can be raised on the geological record they used to define the timing and the triggering mechanism of the PEMR. First, Bowles (2006, 2007) studied in detail the magnetic remanence and the magnetic fabric of ODP Site 1262,

*Now at: Department of Earth and Environmental Science, Ludwig-Maximilians University, Munich D-80333, Germany.

pointing out that the cores have suffered pervasive deformation; in addition, a possible isothermal remanent magnetization acquired during the drilling process may have also contaminated the magnetic directions, making the magnetostratigraphy of the Eocene sediments difficult to interpret. Secondly, the N1(?) polarity event found in the Willwood Formation of the Bighorn Basin by Tauxe *et al.* (1994) was regarded by these authors as of poor reliability because it was based on a single site observation. Thirdly, the presence of short-term normal polarity events reported by Townsend (1985) in calcareous nannofossil zone NP10 within Chron C24r at DSDP Site 550 was more recently rejected by Ali & Hailwood (1998), who reinvestigated the magnetostratigraphy of the same sediment core. Fourthly, Florindo & Roberts (2005) revised the magnetostratigraphy of ODP Site 690 and pointed out that a pervasive overprint is present in the magnetic signal from the middle Eocene downwards, therefore excluding the presence of the short-lived normal polarity events previously reported by Spiess (1990) within Chron C24r. Therefore, as already observed by Flynn & Tauxe (1998) in a review of the available magnetostratigraphic data from upper Palaeocene–lower Eocene marine and terrestrial sediments, there is little evidence of a credible and correlatable normal polarity subchron associated with the Palaeocene/Eocene boundary within Chron C24r.

To resolve the controversy regarding the existence of the PEMR, we discuss (and revise) its supposed duration, and attempt to predict its location in the coeval and well-studied Forada and Cicogna sections of the Belluno Basin in NE Italy (Agnini *et al.* 2007b, Giusberti *et al.* 2007; Dallanave *et al.* 2009, 2010; Fig. 1). We then targeted the PEMR-equivalent levels of these continuous and expanded sections for detailed palaeomagnetic and rock-magnetic analyses.

2 PRESUMED DURATION OF THE PEMR

Röhl *et al.* (2007) developed a cyclostratigraphic age model for the PETM using data from ODP Sites 1262–1265 (Walvis Ridge, South Atlantic Ocean) and Site 690 (Weddel Sea, Southern Ocean). They estimated a total duration of ∼170 kyr for the carbon isotope excursion (CIE) that characterizes the PETM, and a duration of ∼87 kyr for the Clay Layer, which is the lithological expression of the PETM at Walvis Ridge straddling the 'core' of the CIE, within which the PEMR was found at ODP Site 1262 (Lee & Kodama 2009; Fig. 2). Using this age model of sedimentation, we calculated the duration of the PEMR as ∼39 kyr, from 26 to 65 kyr after the onset of the PETM. Our estimate is less than the ∼53 kyr estimate proposed by Lee & Kodama (2009), who used the age model developed by Röhl *et al.* (2000), which was based only on data from ODP Site 690, and was applied to Leg 208 Sites by Zachos *et al.* (2005). Nevertheless, our revised ∼39 kyr duration of the PEMR is still more than four times the maximum duration of any cryptochron described by Cande & Kent (1995) in Chron C24r (∼9 kyr).

3 PETM RECORD OF THE BELLUNO BASIN

Cretaceous to Eocene sediments of the Belluno Basin consist of pelagic to hemipelagic, well-bedded grey to red limestones and marly limestones belonging to the Scaglia Rossa *sensu lato* (*s.l.*) (Di Napoli Alliata *et al.* 1970; Costa *et al.* 1996; Agnini *et al.* 2008). The Palaeocene–Eocene boundary and the associated onset of the negative $\delta^{13}C$ excursion (Fig. 2; Arenillas *et al.* 1999; Giusberti *et al.* 2007) correspond to the base of the so-called clay marl unit (CMU), which consists of ∼0.3–3.4 m of red marly clays and marls representing the lithological expression of the PETM (Arenillas *et al.* 1999; Agnini *et al.* 2006; Giusberti *et al.* 2007; Dallanave *et al.* 2009). The most expanded PETM sections of the Belluno Basin crop out along the Forada stream (Giusberti *et al.* 2007; Agnini *et al.* 2007b) and the nearby Cicogna stream (Dallanave *et al.* 2009, 2010). Common peculiar stratigraphic hallmarks, restricted to the PETM, have been observed in the Forada and Cicogna CMUs as well as in ODP Site 1262, allowing a direct correlation between these sedimentary records. They include (i) a major extinction event among benthic foraminifera (Giusberti *et al.* 2007), (ii) the presence of the calcareous nannofossils excursion taxa (CNET; Aubry *et al.*

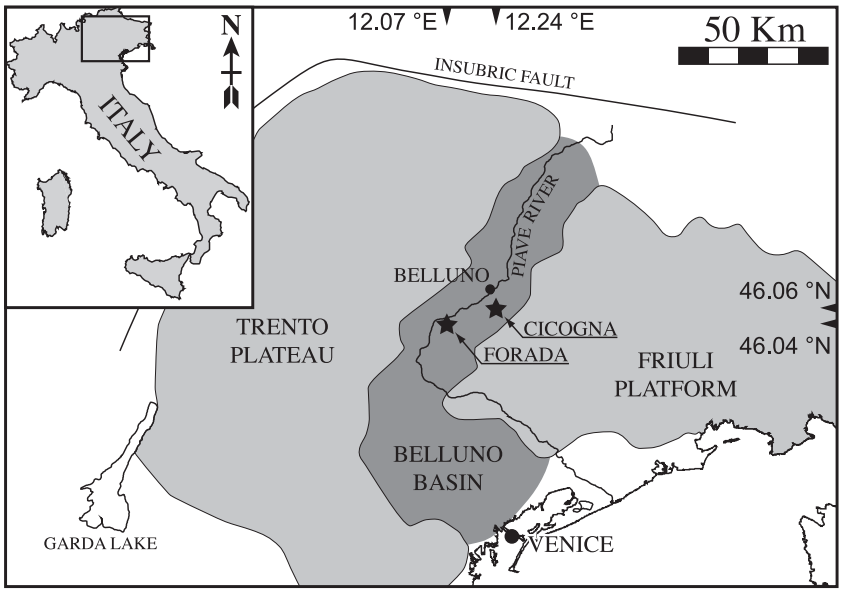

Figure 1. Locations of the Forada and Cicogna Palaeocene–Eocene thermal maximum (PETM) sections (NE Italy); the sections were deposited in the Belluno Basin, a palaeogeographic unit bounded to the west by the Trento Plateau and to the east by the Friuli Platform.

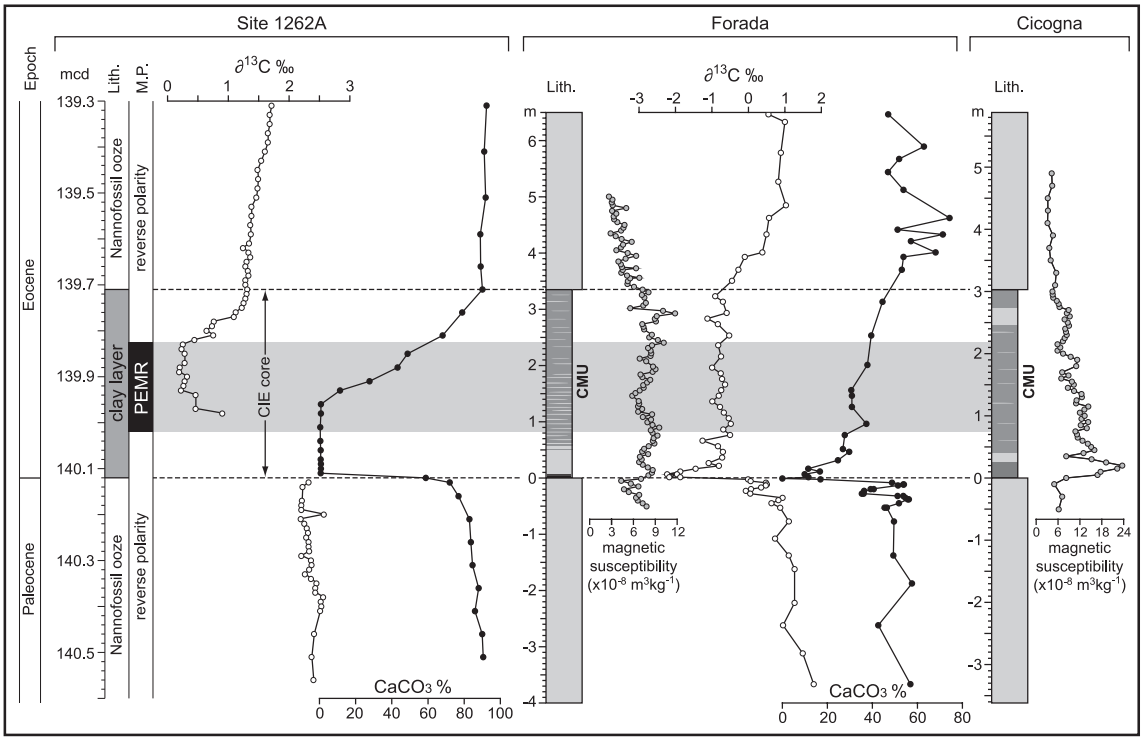

Figure 2. Bulk sediment carbon isotope record and carbonate content for Ocean Drilling Program (ODP) Site 1262A (after Zachos *et al.* 2005) and for the Forada clay marl unit (CMU, after Giusberti *et al.* 2007), placed aside the initial magnetic susceptibility of the Forada and Cicogna CMUs. The main lithology (Lith.) of ODP Site 1262A is plotted against meters of composite depth (mcd) and the magnetic polarity (M.P.) of Lee & Kodama (2009). In the lithology logs of the Forada and Cicogna CMUs, the red and grey-greenish sediments are indicated in dark grey and light grey, respectively (see text for details); zero-metre level indicates the base of the CMU, which at Forada coincides with the base of the global carbon isotope excursion (Giusberti *et al.* 2007). The initial magnetic susceptibility of the Cicogna section is after Dallanave *et al.* (2009). The background grey band indicates the theoretical position on the Forada and Cicogna stratigraphy of the Palaeocene–Eocene magnetic reversal (PEMR) that Lee & Kodama found at ODP Site 1262A.

2002; Agnini *et al.* 2007a,b; Dallanave *et al.* 2009) and (iii) a marked negative δ^{13}C shift (Zachos *et al.* 2005; Giusberti *et al.* 2007).

At Forada (Fig. 2), the base of the CMU is marked by a ∼0.3-cm-thick black clay horizon associated with a spike of biogenic barium and a significant increase in organic carbon (Giusberti *et al.* 2007). Above this horizon are ∼0.5 m of greenish–grey clay marls, finely laminated at the base. From ∼0.5 to ∼1.9 m, the sediments consist of red marls with centimetre-scale grey-greenish spots and lenses. From ∼1.9 m to the CMU top at 3.35 m, the prevalent colour of the sediment is red, although the presence of grey-greenish levels and patches persists.

At Cicogna (Fig. 2), the CMU starts with a ∼25-cm-thick red soft clay level, overlain up to ∼0.4 m by grey-greenish marls. Up to the CMU top at 3.03 m, the sediments are mainly composed of red marls flecked by rare grey-greenish patches; a grey-greenish level is present between 2.46 and 2.72 m. At both sections, the CMU is overlain by Eocene reddish marly limestone–marl couplets.

3.1 Presumed location of the PEMR at Forada and Cicogna

The CIE was likely caused by the rapid release in the ocean-atmosphere system of a large mass (>2000 × 10^9 metric tons) of ^{12}C-enriched carbon (Dickens *et al.* 1995; Zeebe *et al.* 2009). The light carbon released at the onset of the PETM was relatively rapidly cycled throughout the whole ocean-atmosphere system, and the abrupt ∂^{13}C negative excursion was globally recorded across terrestrial, surface-ocean and deep-marine environments within approximately 10 kyr (Dunkley Jones *et al.* 2010). We compared the carbon isotope record at Forada (Giusberti *et al.* 2007) with that from ODP Site 1262. Giusberti *et al.* (2007) used precession-modulated variations of carbonate and haematite concentration, carbon isotopes, and the abundance of calcified radiolaria to determine a duration of ∼105 kyr for the CMU at Forada, which straddles the core of the ∂^{13}C excursion (Fig. 2). Despite differences in age models between Röhl *et al.* (2007) and Giusberti *et al.* (2007) (see Röhl *et al.* 2007 for details), the ∂^{13}C excursion-based correlation between the Clay Layer of ODP Site 1262 and the CMU at Forada allows us to constrain the theoretical position of the PEMR at Forada, which should lie between ∼0.8 and ∼2.4 m from the CMU base. At Cicogna, the PEMR should lie between ∼0.75 and ∼2.2 m from the CMU base, assuming a duration of the CMU similar to that at Forada (Fig. 2).

4 MATERIAL AND METHODS

The rock-magnetic properties of the Cicogna CMU were investigated by Dallanave *et al.* (2010). At Forada, we collected a set of 113 unoriented samples from −0.5 up to 5.0 m, that is, 1.45 m above the CMU top. We first measured the initial magnetic susceptibility of all the specimens. Then, a selected set of 34 specimens (21 in red marls and 13 grey-greenish marls) was magnetized in 2.5, 1.0 and 0.1 T fields along three orthogonal axes. These specimens were subsequently subjected to thermal demagnetization adopting 18 demagnetization steps from room temperature to 670 °C (Lowrie 1990). Hysteresis parameters were obtained by analyzing a suite

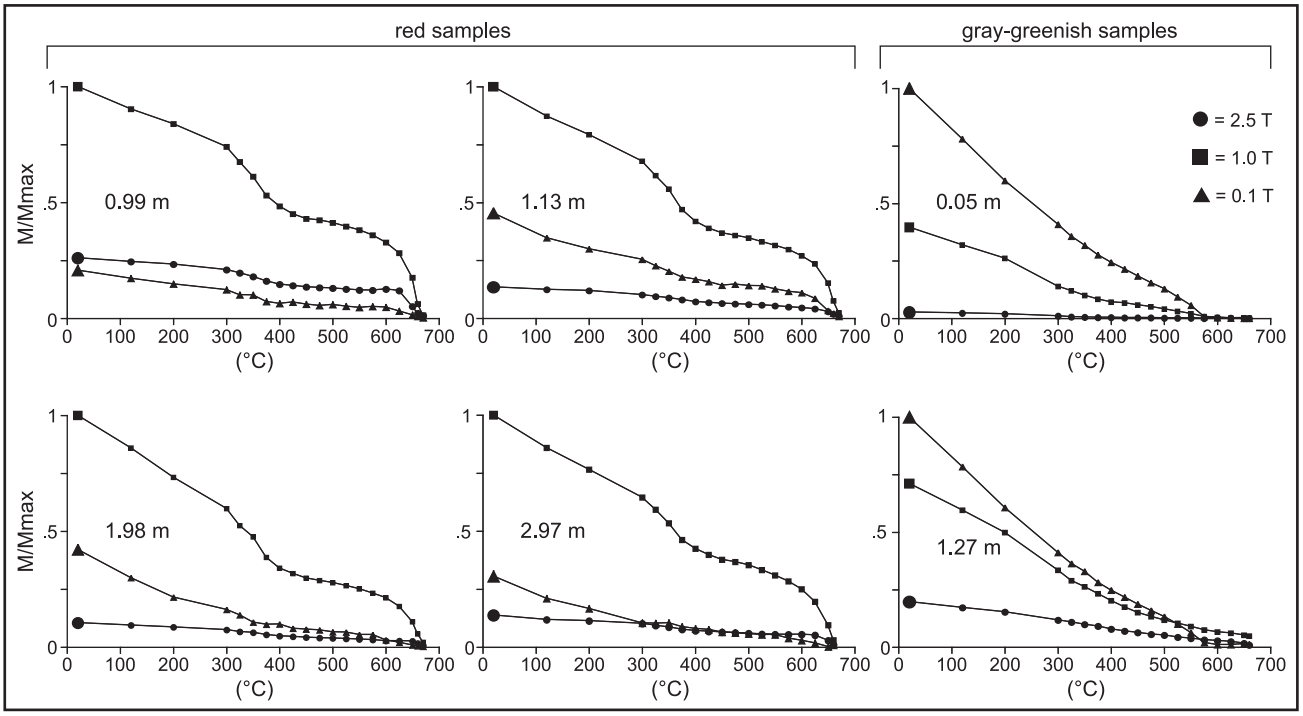

Figure 3. Representative thermal demagnetization data of three-component IRMs imparted to the red and the grey-greenish samples from the Forada section; M/Mmax, magnetization/maximum magnetization.

of 12 ∼0.02–0.03 g specimens with a MICROMAG alternating gradient force magnetometer. Values of saturation magnetization (Ms), saturation remanence (Mr) and coercivity (Bc) were determined from the hysteresis loops after correction for the presence of a ubiquitous paramagnetic component. The values of the coercivity of remanence (Bcr) were estimated by calculating the parameter ΔM obtained by subtracting the ascending (0–1 T) from the descending (1–0 T) branches of the loop, with Bcr approximated by the field value at $\Delta M = 50$ per cent (Tauxe 2010). These analyses were conducted at the palaeomagnetic laboratory of the Scripps Institution of Oceanography (La Jolla, CA, USA).

To determine the magnetic-polarity stratigraphy of the sections, we collected a total number of 51 oriented core samples (19 at Cicogna and 32 at Forada). All the samples were drilled with a portable drill and oriented with a magnetic compass. Each core sample yielded a standard ∼11 cm^3 oriented specimen for natural remanent magnetization (NRM) analysis that was thermally demagnetized up to 670 °C in steps of 50 °C, reduced to 25–15 °C close to critical unblocking temperatures. The component structure of the NRM was examined by means of vector endpoint demagnetization diagrams (Zijderveld 1967). We used the standard least-square analysis of Kirschvink (1980) on linear portions of the demagnetization paths to extract magnetic components, and the statistical analysis of Fisher (1953) to calculate the mean directions and the associated confidence parameters. Thermal demagnetization of the oriented cores was conducted at the Alpine Laboratory of Paleomagnetism (Cuneo, Italy).

5 ROCK-MAGNETISM

Dallanave *et al.* (2010) described the presence in the red sediments of the Cicogna CMU of haematite associated with maghemite. Dominant magnetite, coexisting with minor haematite, characterizes the grey-greenish levels and spots scattered throughout the CMU, which were interpreted as diagenetic in origin. As described below, rock-magnetic data from the Forada CMU confirm this interpretation.

5.1 Forada CMU: red sediments

The magnetic susceptibility ranges between 2 and 12 × 10^{-8} m^3 kg^{-1}, showing generally higher values across the CMU (Fig. 2). Thermal demagnetizations of a three-component IRM are dominated by a 1.0 T coercivity phase that, after a loss of magnetization between 300 and 400 °C, decreases to zero at 670 °C (Fig. 3). This behaviour is generally consistent with the presence of haematite. The smooth decrease between 300 and 400 °C is interpreted as the breakdown of subsidiary maghemite (at the core of haematite grains?) during heating in nearly zero magnetic field (e.g. Kodama 1982; Wang *et al.* 2004), as already observed in the Cicogna CMU (Dallanave *et al.* 2010). The 0.1 T (low) coercivity curve shows instead a progressive intensity decline up to ∼650–670 °C, indicating the presence of pure maghemite characterized by low coercivities and Curie temperatures ranging from 590 to 675 °C (Tauxe 2010) although it could also be a lower coercivity form of haematite (specular haematite) as found by Tauxe *et al.* (1980). A minor 2.5 T (high) coercivity phase with maximum unblocking temperature of ∼670 °C is also present and interpreted as haematite. Hysteresis loops of red sediments (Fig. 4a) have been used to calculate hysteresis parameters, which, when plotted on an Mr/Ms versus Bcr/Bc diagram (Fig. 4b), fall well above the distribution from magnetite-bearing limestones from the literature (Channell & McCabe 1994). The Mr/Ms versus Bcr/Bc distribution generally straddles from reference values of Mr/Ms = 0.6 and Bcr/Bc = 1.5 typical of single-domain haematite to values of Mr/Ms = 0.4 and Bcr/Bc = 4.3 typical of mixtures of single-domain haematite and pseudo-single domain (PSD) magnetite, as suggested by Roberts *et al.* (1995; Fig. 4b). The wasp-waisted shape that characterizes some of the loops (sample 1.84 m of Fig. 4a) also supports the coexistence of

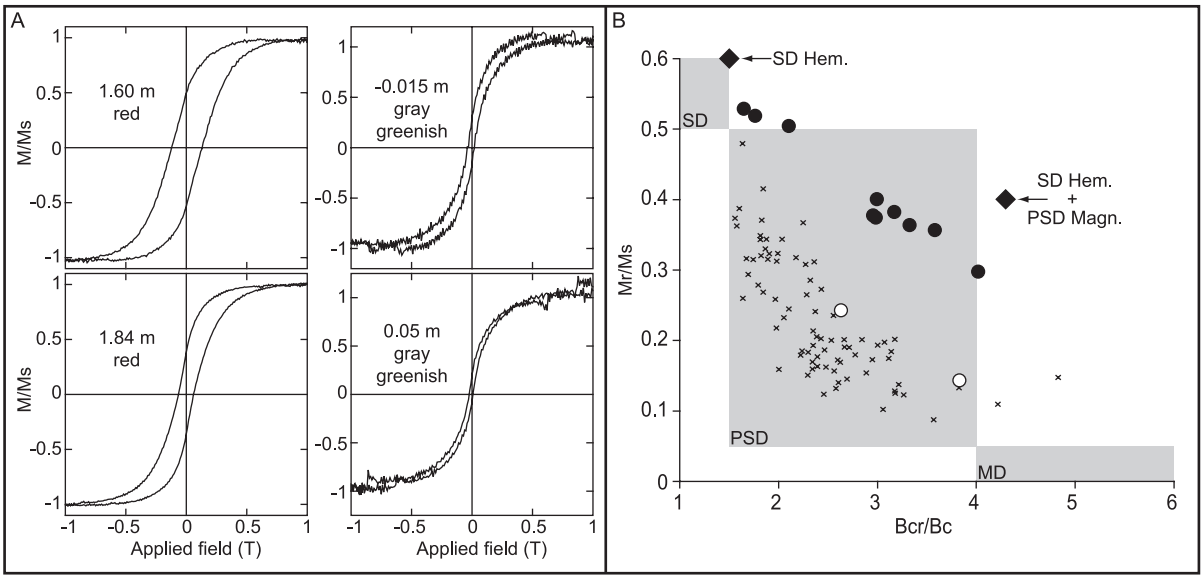

Figure 4. (a) Hysteresis loops of representative red and grey greenish samples from the Forada section, corrected for the paramagnetic component; M/Ms, magnetization/saturation magnetization. (b) Plot of Mr/Ms versus Bcr/Bc (Mr, remanent magnetization; Ms, saturation magnetization; Bcr, coercivity of remanence; Bc, magnetic coercivity) of red (closed circles) and grey-greenish (open circles) specimens from the Forada CMU. The distribution is compared to a reference distribution of hysteresis parameters (black crosses) of magnetite-bearing limestones from the literature (Channell & McCabe 1994). The black diamonds indicate reference values for an SD (single domain) haematite-PSD (pseudo-single domain) magnetite mixture, and for SD haematite (Roberts *et al.* 1995). The grey areas indicate the range of values for SD, PSD and MD (multidomain) magnetite of Day *et al.* (1977).

two distinctive magnetic coercivity fractions (Channell & McCabe 1994; Muttoni 1995; Roberts *et al.* 1995; Tauxe *et al.* 1996).

5.2 Forada CMU: grey-greenish levels and spots

Thermal demagnetization of the three-component IRM from the grey-greenish CMU base at Forada (∼0.0–0.5 m) are dominated by the 0.1 T coercivity phase with a minor 1.0 T phase, both approaching zero at 575 °C and interpreted as due to magnetite; the 2.5 T coercivity phase is virtually absent (Fig. 3, e.g. sample 0.05 m). Upsection, the grey-greenish spots scattered throughout the red CMU are characterized by a similar magnetic mineralogy, albeit here a slightly higher contribution of haematite (1.0 T curve with maximum unblocking temperature of ∼670 °C) is also apparent (Fig. 3, e.g. sample 1.27 m). The low signal-to-noise ratio that generally characterizes the hysteresis loops of these sediments does not allow a reliable determination of the hysteresis parameters, except for two samples from −0.015 and 0.05 m across the CMU lower boundary (Fig. 4a); the Mr/Ms and Bc/Bcr ratios of these samples are similar to the reference values for magnetite-bearing limestone of Channell & McCabe (1994), falling in the region of the plot commonly associated with PSD magnetite (Day *et al.* 1977; Fig. 4b).

6 PALAEOMAGNETISM

6.1 Forada CMU

The intensity of the NRM ranges between 0.01 and 0.38 × 10^{-2} A m^{-1}. Magnetic 'A' component directions statistically oriented N-and-down in geographic coordinates have been observed in all samples from room temperature up to 250–300 °C (Fig. 5; Tables 1 and A1). After removal of this overprint component, approximately oriented along the present-day field direction (Fig. 6a), three types of behaviour were observed. Three samples collected in the basal grey-greenish interval of the section, from −0.1 to 0.5 m, show a characteristic remanent magnetization (ChRM) component-oriented S-and-up in geographic coordinates and linearly trending to the origin of the demagnetization axes up to 575 °C (Fig. 5, fr01); this component is interpreted as carried by magnetite. In 15 of the remaining 29 red samples, the 'A' component is followed by a 'B' component isolated up to an average unblocking temperature of ∼600 °C, and roughly directed NE-and-down in geographic coordinates (Fig. 5, fr05, fr24, fr27; Fig. 6a; Tables 1 and A1). These highly scattered 'B' directions can be speculatively interpreted as a due to the secondary growth of pigmentary haematite, which typically possess unblocking temperatures lower than those of detrital haematite (Tauxe *et al.* 1980). These 'B' component directions are followed up to 670 °C by S-and-up ChRM component directions interpreted as carried by haematite. In the remainder of the specimens (14), the 'A' component is directly followed by the S-and-up ChRM haematitic component, isolated up to 670 °C (Fig. 5, fr12, fr15). The characteristic ChRM directions of the Forada CMU are well clustered and all oriented S-and-Up in geographic coordinates; after correction for homoclinal bedding tilt, the average ChRM direction becomes ∼7° shallower while maintaining a S-and-up orientation (Fig. 6a; Tables 1 and A1).

6.2 Cicogna CMU

The intensity of the NRM ranges between 0.03 and 0.7 × 10^{-2} A m^{-1}. Highly scattered, generally downpointing 'A' component directions broadly oriented along the present-day field direction were isolated between room temperature and 200–250 °C (Figs 5 and 6b; Tables 1 and A1). After removal of these directions, all samples showed a stable characteristic ChRM magnetization linearly trending to the origin of the demagnetization axes and isolated

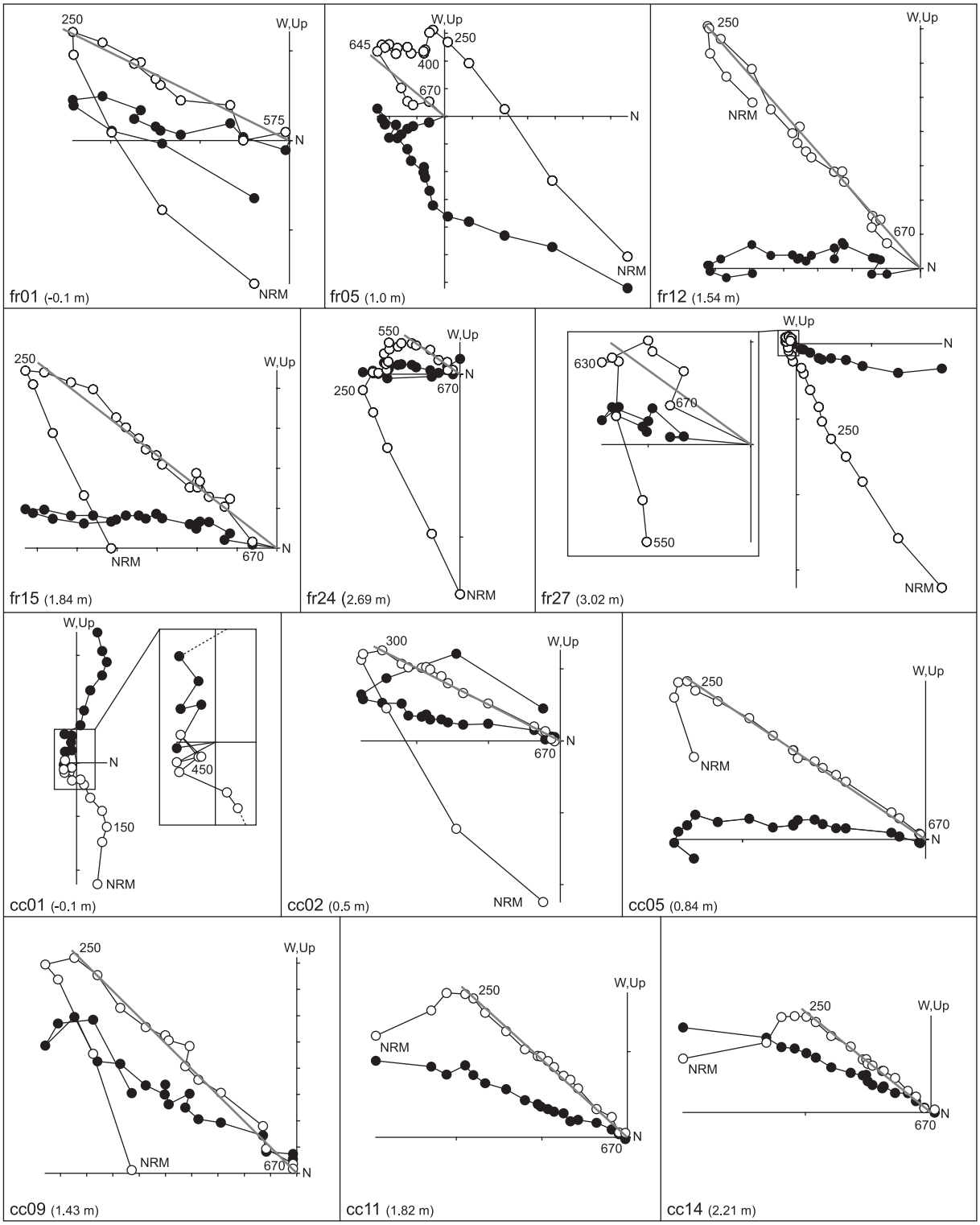

Figure 5. Vector endpoint demagnetization diagrams of the natural remanent magnetization (NRM) of representative oriented cores from the CMU at Forada (samples fr01–fr27) and Cicogna (samples cc01–cc14), with indication of the stratigraphic position of samples in metres from the CMU base. Closed (open) circles are projections onto the horizontal (vertical) plane in geographic coordinates; the grey thick lines indicate the ChRM components.

up to 670 °C. This unblocking temperature suggests, together with previous rock-magnetic data (Dallanave *et al.* 2010), that this ChRM magnetization is carried by haematite. Only a single grey sample collected at −0.1 m, that is, before the onset of the PETM (Fig. 2), shows an intermediate component direction (B?) isolated up to 450 °C and oriented WNW-and-down in geographic coordinates (Fig. 5, cc01; Fig. 6b). All ChRM directions are well-clustered and oriented SSW-and-up in geographic coordinates, turning to a shallower S-and-up orientation after correction for bedding tilt (Fig. 6b; Tables 1 and A1).

Table 1. Magnetic component directions from the Forada and Cicogna clay marl unit (CMU) sections.

Comp.	MAD	*N*	Geographic coordinates				Tilt-corrected coordinates			
			k	α95	Dec	Inc	*k*	α95	Dec	Inc
fr A	5.1 ± 2.4	32	15.4	6.7	10.1	55.1				
fr B	11.9 ± 6.0	15	3.9	22.4	36.2	52.1				
fr ChRM	7.7 ± 4.1	32	20.3	5.8	186.6	−39.1	20.3	5.8	187.5	−25.1
cc A	8.4 ± 3.7	19	4.3	18.5	251.6	74.6				
cc ChRM	4.3 ± 3.1	18	25.3	7.0	201.1	−37.3	25.3	7.0	183.8	−10.3

Notes. fr, Forada; cc, Cicogna; *N*, number of directions; MAD, maximum angular deviation (°); *k*, Fisher (1953) precision parameter of the mean palaeomagnetic direction; α95, Fisher angle (°) of half cone of 95 per cent of confidence about the mean palaeomagnetic direction; Dec and Inc, declination and inclination of the mean palaeomagnetic direction (°E and °, respectively).

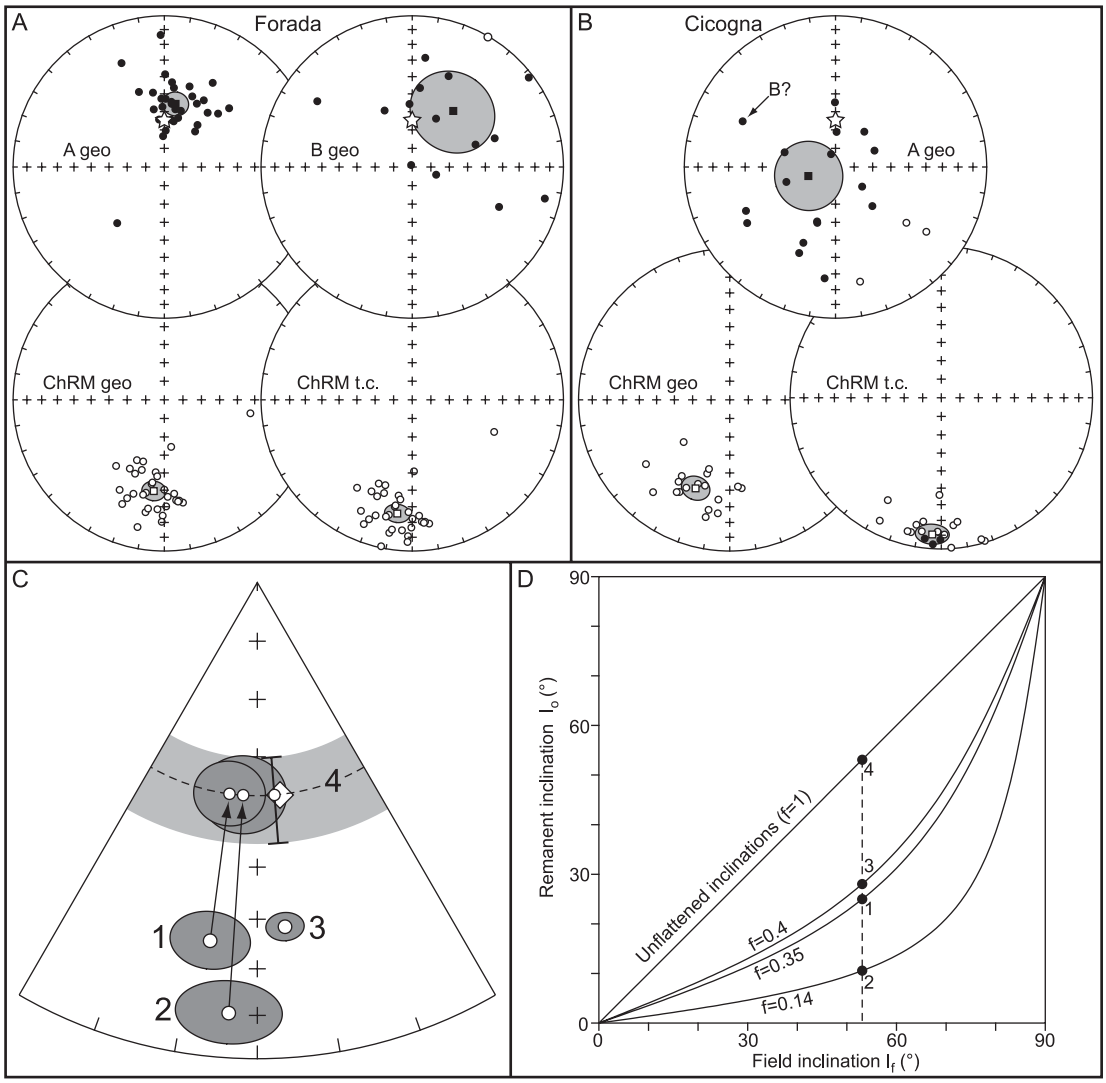

Figure 6. Equal area stereographic projections of the 'A', 'B', and ChRM components of the Forada (a) and Cicogna (b) sediments; geo and t.c. indicate geographic and tilt-corrected coordinates, respectively. Closed (open) symbols represent down-pointing (up-pointing) directions. The grey circles represent the α_{95} cone of confidence around the mean directions (squares) (Fisher 1953). White stars represent the present-day geomagnetic field direction calculated using the geocentric axial dipole (GAD; Tauxe 2010) field model. (c) The average ChRM directions and α_{95} cones of confidence of the Forada (1) and Cicogna (2) clay marl unit (CMU) are compared with the previously published mean direction from pre- and post-CMU strata at Cicogna plotted both before (3) and after (4) correction for inclination shallowing (Dallanave *et al.* 2009), as well as with the expected magnetic direction at the sampling sites calculated using the 55 Ma African palaeopole of the Besse & Courtillot (2003) (white diamond). (d) Plot of the remanent inclination (I_0) versus inducing field inclination (I_f) accordingly to the equation $\tan I_0 = f \tan I_f$ proposed by King (1955); closed circles 1–3 represent, respectively, the average ChRM inclination of the Forada CMU, the Cicogna CMU and the overall (late Palaeocene–early Eocene) Cicogna section embracing the homonymous CMU (Dallanave *et al.* 2009). The E/I (elongation/inclination; Tauxe & Kent 2004) corrected inclination of the overall Cicogna section of Dallanave *et al.* (2009) (−53.1°, closed circle 4) is used as reference unflattened inclination to calculate the flattening factors '*f*' of the Cicogna and Forada CMU mean directions (0.35 and 0.14, respectively); see text for details.

7 DISCUSSIONS

7.1 Inclination shallowing

Dallanave *et al.* (2009) found that the late Palaeocene–early Eocene Cicogna section (save for the CMU that was not sampled) is affected by inclination shallowing, which they corrected by applying the E/I (elongation/inclination) statistical method of Tauxe & Kent (2004; see also Kent & Tauxe 2005; Tauxe *et al.* 2008). After correction, they obtained an average magnetic direction (Dec. = 175.4°; Inc. = −53.1°) that is virtually indistinguishable from the expected direction derived from the coeval palaeopole (∼55 Ma) of the African apparent polar wander path (APWP) of Besse & Courtillot (2002, 2003; BC03) (Fig. 6c; see Dallanave *et al.* 2009 for details). The corrected inclination (Inc. = −53.1°) is here used as reference value to estimate inclination shallowing in the Forada (Inc. = −25.1°) and Cicogna (Inc. = −10.3°) CMUs, where sampling density is insufficient to carry out a proper E/I test.

We estimated inclination anomalies of approx. −28° at Forada and of approx. −43° at Cicogna, corresponding to flattening factors (f) of 0.35 and 0.14, respectively; f is calculated by $f = \tan I_0/\tan I_f$ (where I_0 and I_f are the remanent inclination and the true inclination of the magnetic field during sedimentation, respectively; King 1955). The reference inclination of −53.1° is assumed to lie on the $f = 1$ line (no shallowing) for comparison with the curves corresponding to $f = 0.35$ (Forada CMU) and $f = 0.14$ (Cicogna CMU) (Fig. 6d). The f values of the Cicogna and Forada CMUs are found to be among the lowest ever measured in sediments; they are lower than values of 0.4 and 0.5 for, respectively, strata below and above the CMU at Cicogna (Dallanave *et al.* 2009), and strata of Late Cretaceous–early Eocene age from the nearby South Ardo section (Dallanave *et al.* 2012). They are also lower than values of about 0.4 for recent river-laid deposits containing detrital haematite (Tauxe & Kent 1984). This extreme degree of shallowing is speculatively due to the combination of depositional inclination flattening, typical of the detrital haematite, and post-depositional compaction of clays, which are particularly abundant in the carbonate-depleted CMU. Tan *et al.* (2002) found experimentally that during shallow (<100 m) burial compaction, clay-size sediments containing detrital haematite particles can experience a magnetic inclination shallowing of 17°–19° starting from an induced inclination of 58°. For increasingly higher burial depths, which are usually associated with increasingly older sediments, compaction-derived inclination flattening tends to increase accordingly (Tan *et al.* 2002). The difference in degree of flattening between the Forada CMU ($f = 0.35$) and the Cicogna CMU ($f = 0.14$) can be attributed to different compaction degrees of sediments with slightly different composition. The Cicogna CMU is ∼10 per cent thinner than the Forada CMU, and is generally characterized by higher magnetic susceptibility values (Fig. 2) possibly indicating higher clay mineral and detrital haematite concentration due to higher carbonate matrix dissolution; we speculate that these lithological characteristics (higher amount of flattenable clay and haematite grains) may have resulted in a more pronounced degree of flattening of the ChRM directions in the Cicogna CMU relative to the Forada CMU.

7.2 Origin of the magnetic particles

The haematite observed in the red sediments of the Forada and Cicogna CMUs carries primary magnetic directions affected by a strong inclination shallowing and is thus interpreted as primary as well as detrital in origin. The grey-greenish levels and spots

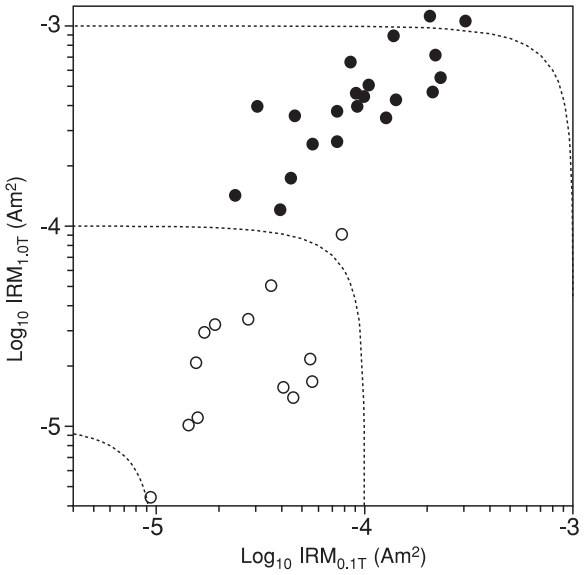

Figure 7. Logarithmic plot of the IRM at 0.1 and 1.0 T for representative red and grey-greenish samples; dotted lines represent equal IRM intensities. Grey-greenish samples (open circles) show generally low IRM values compared to red samples (closed circles); see text for details. [Correction made after online publication 2012 September 20: this figure has been corrected and the caption has been reworded accordingly.]

scattered through the red CMU are instead interpreted as the loci of post-depositional transformation of primary haematite and/or maghemite into magnetite under localized reducing diagenetic conditions (e.g. Özdemir & Dunlop 1988; Torrent *et al.* 2010), followed by the progressive dissolution of the newly formed magnetite under persistent reducing conditions (Fischer *et al.* 2007); this is supported by the very low IRM intensities of these grey-greenish levels and spots compared to the surrounding red sediments (Fig. 7). The samples collected in the Forada grey-greenish level from −0.1 to 0.5 m have been previously shown to contain magnetite that carries a primary reverse polarity magnetization; this supports the hypothesis that the reducing conditions were established soon after sediment deposition, possibly sometime during the ∼1.5-Myr-long interval of Chron C24r following the CMU onset.

7.3 Is there a normal magnetic-polarity event during the PETM?

We calculated the position of the virtual geomagnetic pole (VGP) for each ChRM direction along the Forada and Cicogna CMUs to outline the magnetic-polarity stratigraphy. The latitude of each sample VGP relative to the mean palaeomagnetic (north) pole axis was used for interpreting polarity stratigraphy. Relative VGP latitudes approaching 90°N (90°S) are interpreted as recording normal (reverse) polarity (Fig. 8). Data reveal that both the Forada and Cicogna CMU sediments were deposited during a continuous reverse magnetic-polarity interval, which, according to previous magnetostratigraphic and biostratigraphic data (Agnini *et al.* 2007b; Dallanave *et al.* 2009), can unequivocally be attributed to Chron C24r (∼53.3–55.9 Ma; Cande & Kent 1995).

If no normal magnetic-polarity event occurred during the PETM, what is the origin of the normal magnetic-polarity directions recorded in the Clay Layer of ODP Site 1262? Numerous ODP and DSDP palaeomagnetic studies have documented the presence of a magnetic overprint associated with an IRM imparted to the

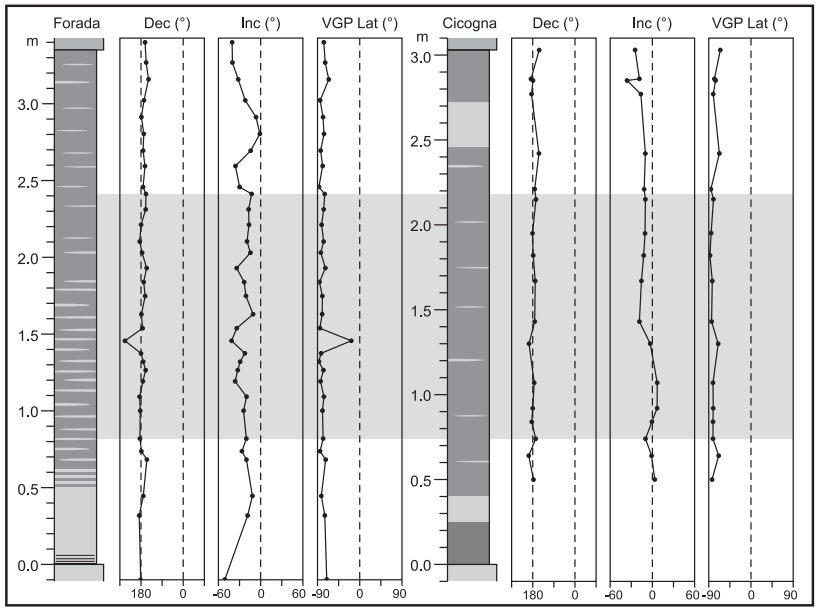

Figure 8. Magnetic logs of the Forada and Cicogna clay marl units (CMUs) showing the natural remanent magnetization (NRM) values, the declination and inclination of the characteristic component directions, and the derived virtual geomagnetic pole latitudes. The grey band highlights the theoretical position of the Palaeocene–Eocene magnetic reversal (PEMR), which was not observed at Forada and Cicogna.

core during drilling and/or splitting operations. Magnetic field measurements have indicated that the fields generated near the drilling equipment are generally less than ∼20 mT, even though they can locally exceed 1 T (Acton *et al.* 2002 and references therein). This seems to be the case at least for some of the ODP Site 1262 sediments for which a general magnetic declination bias likely produced by an IRM acquired during or after drilling has been reported (Bowles 2006, 2007), and the magnetic inclination data appear to be quite scattered above the Palaeocene/Eocene boundary. Bearing this in mind, we speculate that the normal polarity magnetic components documented by Lee & Kodama (2009, online material) from the Clay Layer at ODP Site 1262, which were isolated up to only 20 mT and never down to the origin of the demagnetization axes, could represent drilling-induced remagnetizations of normal polarity. The tight connection between lithology (Clay Layer) and magnetic polarity (PEMR) documented by Lee and Kodama adds further doubt to the PEMR hypothesis; this Clay Layer is enriched in maghemite compared to underlying and overlying levels (Lee & Kodama 2009), a mineral that can originate from low temperature oxidation of (primary) magnetite, and can therefore easily carry a late-acquired magnetic overprint (Kent & Lowrie 1974).

8 CONCLUSIONS

We conducted a detailed palaeomagnetic study of the Forada and the Cicogna CMUs to confirm (or refute) the existence of the short normal polarity event (PEMR) reported by Lee & Kodama (2009) in the correlative Clay Layer of ODP Site 1262 straddling the core of the PETM global $\partial^{13}C$ excursion. These authors interpreted the PEMR as triggered by a perturbation of the Earth's rotation rate related to a change in the oceanic-atmospheric circulation patterns that took place during the PETM. However, our data set revealed that no magnetic-polarity reversals occurred throughout the CMU interval (= core of the $\partial^{13}C$ excursion) in the Belluno Basin. The CMU at Forada is consistently characterized by reverse magnetic polarity, which we resolved temporally down to an average of ∼3.3 kyr (minimum of ∼1.5 kyr) using the age model of CMU deposition of Giusberti *et al.* (2007). Although we cannot rule out the existence in the studied sections of extremely short (< ∼1.5 kyr long) polarity excursions, our findings demonstrate a substantial lack of connection between the CMU as a lithological expression of the PETM and magnetic-polarity reversals.

Extremely flattened magnetic component directions carried by haematite have been observed at both sections; this large inclination error, characterized by flattening values down to $f = 0.14$, is due to the presence in the red CMU of abundant detrital haematite, which frequently acquires a magnetic remanence shallower than the inducing field (e.g. Tauxe & Kent 1984), coupled with the post-depositional compaction of the clay-rich and carbonate-depleted CMU sediments. This abundant detrital haematite may have originated as a consequence of the warm and humid climate conditions typical of the PETM that enhanced continental weathering of silicates on land and the consequent production, transport and sedimentation of oxidized Fe phases, as suggested by Dallanave *et al.* (2010; and references therein). The magnetite-dominated mineralogy of the grey-greenish levels and spots scattered within the CMU is interpreted as early diagenetic in origin. Palaeomagnetic data, albeit limited to the Forada CMU base, suggest that diagenetic reduction took place soon after sediment deposition, causing the newly formed magnetite to acquire a reverse magnetization consistent with the direction carried by the primary detrital haematite of the surrounding red sediments. In conclusion, although we see how climate can exert a strong forcing on the oxidation state of the iron oxides entering a sedimentary basin as detrital phases, we cannot see how it could control the convection in the outer core and trigger magnetic-polarity reversals.

ACKNOWLEDGMENTS

Two anonymous reviewers are warmly thanked for comments that greatly improved this manuscript. We thank Luca Giusberti for the fruitful discussion. The SIO lab was funded in part by NSF grant # OCE1058858. ED, CA, and DR were supported by the University of Padova.

REFERENCES

Acton, G.D., Okata, M., Clement, B.M., Lund, S.P. & Williams, T., 2002. Paleomagnetic overprints in ocean sediment cores and their relationship to shear deformation caused by piston coring, *J. geophys. Res.,* **107**(B4), doi:10.1029/2001JB000518.

Agnini, C., Muttoni, G., Kent, D.V. & Rio, D., 2006. Eocene biostratigraphy and magnetic stratigraphy from Possagno, Italy: the calcareous nannofossils response to climate variability, *Earth planet. Sci. Lett.,* **241,** 815–830.

Agnini, C., Fornaciari, E., Raffi, I., Rio, D., Röhl, U. & Westerhold, T., 2007a. High-resolution nannofossil biochronology of middle Paleocene to early Eocene at ODP Site 1262: implications for calcareous nannoplankton evolution, *Mar. Micropal.,* **64,** 215–248.

Agnini, C., Fornaciari, E., Rio, D., Tateo, F., Backman, J. & Giusberti, L., 2007b. Responses of calcareous nannofossil assemblage, mineralogy and geochemistry to the environmental perturbations across the Paleocene/Eocene boundary in the Venetian Pre-Alps, *Mar. Micropal.,* **63,** 19–38.

Agnini, C. *et al*., 2008. Il Paleogene inferiore in facies pelagica del Veneto nord-orientale, *Rend. Soc. Geol. It.,* **4,** 5–12.

Ali, J.R. & Hailwood, E.A., 1998. Magnetostratigraphic (re)calibration of the Paleocene/Eocene boundary interval in Holes 550 and 549, Goban Spur, eastern North Atlantic, *Earth planet. Sci. Lett.,* **161,** 201–213.

Arenillas, I., Molina, E. & Schmitz, B., 1999. Planktic foraminiferal and $\partial^{13}C$ isotopic changes across the Paleocene/Eocene boundary at Possagno (Italy), *Int. J. Earth Sci.,* **88,** 352–364, doi:1007/s005310050270.

Aubry, M.-P. *et al.*, 2002. Global standard stratotype-section and point (GSSP) at the Dababiya section (Egypt) for the Base of the Eocene Series, *Episodes,* **30**(4), 271–286.

Besse, J. & Courtillot, V., 2002. Apparent and true polar wander and the geometry of the geomagnetic field over the last 200 Myr, *J. geophys. Res.,* **107**(B11), 2300, doi:10.1029/2000JB000050.

Besse, J. & Courtillot, V., 2003. Correction to 'Apparent and true polar wander and the geometry of the geomagnetic field over the last 200 Myr', *J. geophys. Res.,* **108**(B10), 2469, doi:10.1029/2003JB002684.

Bowles, J., 2006. Revised magnetostratigraphy and magnetic mineralogy of sediments from Walvis Ridge, Leg 208, *Proc. Ocean Drill. Prog., Sci. Results,* **208,** 1–24, doi:10.2973/odp.proc.sr.208.206.2006.

Bowles, J., 2007. Coring-related deformation of Leg 208 sediments from Walvis Ridge: implications for paleomagnetic data, *Phys. Earth planet. Inter.,* **16,** 161–169, doi:10.1016/j.pepi.2007.01.010.

Cande, S.C. & Kent, D.V., 1992a. A new geomagnetic polarity time scale for the Late Cretaceous and Cenozoic, *J. geophys. Res.,* **97,** 13 917–13 951.

Cande, S.C. & Kent, D.V., 1992b. Ultra-high resolution marine magnetic anomaly-profiles: a record of continuous paleointensity variations? *J. geophys. Res.,* **97,** 15 075–15 083.

Cande, S.C. & Kent, D.V., 1995. Revised calibration of the geomagnetic polarity time scale for the Late Cretaceous and Cenozoic, *J. geophys. Res.,* **100**(B4), 6093–6096, doi:10.1029/94JB03098.

Channell, J.E.T. & McCabe, C., 1994. Comparison of magnetic hysteresis parameters of unremagnetized and remagnetized limestones, *J. geophys. Res.,* **99**(B3), 4613–4623.

Costa, V., Doglioni, C., Grandesso, P., Masetti, D., Pellegrini, G.B. & Tracanella, E., 1996. *Carta Geologica d'Italia, Foglio 063, Belluno,* Servizio Geologico d'Italia, Roma, 1 sheet + 74 pp.

Dallanave, E., Agnini, C., Muttoni, G. & Rio, D., 2009. Magnetobiostratigraphy of the Cicogna section (Italy): implications for the late Paleocene–early Eocene time scale, *Earth planet. Sci. Lett.,* **285,** 39–51, doi:10.1016/j.epsl.2009.05.033.

Dallanave, E., Tauxe, L., Muttoni, G. & Rio, D., 2010. Silicate weathering machine at work: rock magnetic data from the late Paleocene–early Eocene Cicogna section, Italy, *Geochem. Geophys. Geosyst.,* **11**(7), Q07008, doi:10.1029/2010GC003142.

Dallanave, E., Agnini, C., Muttoni, G. & Rio, D., 2012. Paleocene magnetobiostratigraphy and climate-controlled rock magnetism from the Belluno Basin,Tethys Ocean, Italy, *Palaeogeogr. Palaeoclimatol. Palaeoecol.,* **337–338,** 130–142, doi:10.1016/j.palaeo.2012.04.007.

Day, R., Fuller, M. & Schmidt, V.A., 1977. Hysteresis properties of titanomagnetite: grain-size and compositional dependence, *Phys. Earth planet. Inter.,* **13,** 260–267.

Dickens, G.R., O'Neil, J.R., Rea, D.K. & Owen, R.M., 1995. Dissociation of oceanic methane hydrate as a cause of the carbon isotope excursion at the end of the Paleocene, *Paleoceanography,* **10,** 965–971, doi:10.1029/95PA02087.

Di Napoli Alliata, E., Proto Decima, F. & Pellegrini, G.B., 1970. Studio Geologico, Stratigrafico e Micropaleontologico dei Dintorni di Belluno, *Mem. Soc. Geol. It.,* **9,** 1–28.

Dunkley Jones, T., Ridgwell, A., Lunt, D.J., Maslin, M.A., Schmidt, D.N. & Valdes, P.J., 2010. A Paleogene perspective on climate sensitivity and methane hydrate instability, *Phil. Trans. R. Soc. A.,* **368,** 2395–2415, doi:10.1098/rsta.2010.0053.

Fischer, H., Lustre, J. & Gehring, A.U., 2007. EPR evidence for maghemitization of magnetite in a tropical soil, *Geophys. J. Int.,* **169,** 909–916.

Fisher, R.A., 1953. Dispersion on a sphere, *Proc. R. Soc. Lond. A,* **217,** 295–305.

Florindo, F. & Roberts, A.P., 2005. Eocene–Oligocene magnetobiochronology of the ODP Sites 689 and 690, Maud Rise, Weddel Sea, Antarctica, *Bull. geol. Soc. Am.,* **117**(1/2), 46–66, doi:10.1130/B25541.1.

Flynn, J.J. & Tauxe, L., 1998. Magnetostratigraphy of Upper Paleocene-Lower Eocene marine and terrestrial sequences, in *Late Paleocene-Early Eocene Events,* pp. 98–37, eds Aubry, M.-P., Lucas, S.G. & Berggren, W.A., Columbia University Press, New York, NY.

Giusberti, L., Rio D., Agnini, C., Backman, J., Fornaciari, E., Tateo, F. & Oddone, M., 2007. Mode and tempo of the Paleocene-Eocene thermal maximum in an expanded section from the Venetian pre-Alps, *Bull. geol. Soc. Am.,* **119,** 391–412, doi:10.1130/B25994.1.

Kent, D.V. & Lowrie, W., 1974. Origin of magnetic instability in sediment cores from the Central North Pacific, *J. geophys. Res.,* **79**(20), 2987–3000.

Kent, D.V. & Tauxe, L., 2005. Corrected Late Triassic latitudes for continents adjacent to the North Atlantic, *Science,* **307,** 240–244.

King, R.F., 1955. The remanent magnetism of artificially deposited sediments, *Mon. Not. R. astr. Soc. Geophys. Suppl.,* **7,** 115–134.

Kirschvink, J.L., 1980. The least-squares line and plane and analysis of paleomagnetic data, *Geophys. J. R. astr. Soc.,* **62,** 699–718.

Kodama, K.P., 1982. Magnetic effects of maghemitization of Plio-Pleistocene marine sediments, Northern California, *J. geophys. Res.,* **87**(B8), 7113–7125.

Lee, Y.S. & Kodama, K., 2009. A possible link between the geomagnetic field and catastrophic climate at the Paleocene–Eocene thermal maximum, *Geology,* **37**(11), 1047–1050, doi:10.1130/G30190A.1.

Lowrie, W., 1990. Identification of ferromagnetic minerals in a rock by coercivity and unblocking temperature properties, *Geophys. Res. Lett.,* **17,** 150–162.

Muttoni, G., 1995. 'Wasp-waisted' hysteresis loops from a pyrrhotite and magnetite-bearing remagnetized Triassic limestone, *Geophys. Res. Lett.,* **22**(23), 3167–3170.

Nunes, F. & Norris, R.D., 2006. Abrupt reversal in ocean overturning during the Paleocene/Eocene warm period, *Nature,* **439,** 60–63, doi:10.1038/nature04386.

Özdemir, Ö. & Dunlop, D.J., 1988. Crystallization remanent magnetization during the transformation of maghemite to hematite, *J. geophys. Res.,* **93**(B6), 6530–6544.

Roberts, A.P., Cui, Y. & Verosub, K.L., 1995. Wasp-waisted hysteresis loops: mineral characteristic and discrimination of components in mixed magnetic systems, *J. geophys. Res.,* **100**(B9), 17 909–17 924.

Röhl, U., Bralower, T.J., Norris, R.D. & Wefer, G., 2000. New chronology for the late Paleocene thermal maximum and its environmental implications, *Geology,* **28**(10), 927–930.

Röhl, U., Westerhold, T., Bralower, T.J. & Zachos, J.C., 2007. On the duration of the Paleocene–Eocene thermal maximum (PETM), *Geochem. Geophys. Geosyst.,* **8**(12), doi:10.1029/2007GC001784.

Spiess, V., 1990. Cenozoic magnetostratigraphy of Leg 113 drill sites, Maud Rise, Weddel Sea, Antarctica, *Proc. Ocean Drill. Prog., Sci. Results,* **113,** 261–315, doi:10.2973/odp.proc.sr.113.182.1990.

Tan, X., Kodama, K.P. & Fang, D., 2002. Laboratory depositional and compaction-caused inclination carried by hematite and their implications in identifying inclination error of natural remanence in red beds, *Geophys. J. Int.,* **151,** 475–486.

Tauxe, L., 2010. *Essentials of Paleomagnetism,* Univ. California Press, Berkeley, CA.

Tauxe, L. & Kent, D.V., 1984. Properties of detrital remanence carried by hematite from study of modern river deposits and laboratory redeposition experiments, *Geophys. J. R. astr. Soc.,* **76,** 543–561.

Tauxe, L. & Kent, D.V., 2004. A simplified statistical model for the geomagnetic field and the detection of shallow bias in paleomagnetic inclinations: was the ancient magnetic field dipolar? in *Timescales of the Paleomagnetic Field,* Geophys. Monogr. 145, eds Channell, J.E.T., Kent, D.V., Lowrie, W. & Meert, J.G., American Geophysical Union, Washington, DC.

Tauxe, L., Kent, D.V. & Opdike, N.D., 1980. Magnetic components contributing to the NRM of Middle Siwalik red beds, *Earth planet. Sci. Lett.,* **47,** 279–284.

Tauxe, L., Gee, J., Gallet, Y., Pick, T. & Bown, T., 1994. Magnetostratigraphy of the Willwood Formation, Bighorn Basin, Wyoming: new constraints on the location of the Paleocene/Eocene boundary, *Earth planet. Sci. Lett.,* **125,** 159–172, doi:10.1016/0012-821X(94)90213-5.

Tauxe, L., Mullender, T.A.T. & Pick, T., 1996. Potbellies, wasp-waists, and superparamagnetism in magnetic hysteresis, *J. geophys. Res.,* **101**(B1), 571–583.

Tauxe, L., Kodama, K.P. & Kent, D.V., 2008. Testing for paleomagnetic inclination error in sedimentary rocks: a comparative approach, *Phys. Earth planet. Inter.,* **169,** 152–165.

Torrent, J., Liu, Q.S. & Barrón, V., 2010. Magnetic susceptibility changes in relation to pedogenesis in a Xeralf chronosequence in northwestern Spain, *Eur. J. Soil Sci.,* **61,** 161–173, doi:10.1111/j.1365-2389.2009.01216.x.

Townsend, H.A., 1985. The paleomagnetism of sediments acquired from the Goban Spur on DSDP Leg 80, in *Deep Sea Drilling Project, Initial Reports,* Vol. 80, pp. 389–414, ed Bailey, M.G., U.S. Government Printing Office, Washington, DC.

Wang, X., Yang, Z., Løvlie, R. & Min, L., 2004. High-resolution magnetic stratigraphy of fluvio-lacustrine succession in the Nihewan Basin, China, *Quat. Sci. Rev.,* **23,** 1187–1198.

Zachos, J.C., Pagani, M., Sloan, L., Thomas, E. & Billups, K., 2001. Trends, rythms and aberrations in global climate 65 Ma to present, *Science,* **292,** 686–693.

Zachos, J.C. *et al*., 2004. *Proc. Ocean Drill. Prog., Init. Rep.,* **208,** doi:10.2973/odp.proc.ir.208.2004.

Zachos, J.C. *et al*., 2005. Rapid acidification of the ocean during the Paleocene–Eocene thermal maximum, *Science,* **308,** 1611–1615.

Zeebe, R.E., Zachos, J.C. & Dickens, J.R., 2009. Carbon dioxide forcing alone insufficient to explain Paleocene-Eocene thermal maximum warming, *Nature Geosci.,* **2,** 576–580, doi:10.1038/ngeo578.

Zijderveld, J.D.A., 1967. A.C. demagnetization of rocks: analysis of results, in *Methods in Paleomagnetism,* pp. 254–286, eds Collinson, D.W., Creer, K.M. & Runcorn, S.K., Elsevier, Amsterdam.

APPENDIX

Table A1. Details of the magnetic components of samples form the Cicogna and the Forada clay marly unit (CMU) sections.

Sample	Comp.	*N*	Anch.	MAD	GDECL	GINCL	BDECL	BINCL	Low T	High
fr-01	A	4	no	7.8	358.4	13.7	358.9	0.1	0	200
fr-01	ChRM	7	yes	11.8	171.7	−64.3	178.6	−50.9	200	475
fr00	A	5	no	5.1	11.6	64.8	12.1	50.8	0	250
fr00	ChRM	11	yes	4.3	169.7	−31.5	172.2	−18.5	250	600
fr01	A	5	no	7.0	27.2	51.1	24.2	37.4	0	250
fr01	ChRM	10	yes	4.6	189.5	−25.6	189.8	−11.7	250	575
fr02	A	5	no	10.7	337.6	26.6	340.6	14.9	0	250
fr02	ChRM	18	yes	4.1	206.4	−33.9	204.8	−20.2	250	670
fr03	A	6	no	5.1	30.6	47.5	27.3	34.0	0	300
fr03	B	11	no	13.1	103.4	10.8	100.8	10.6	300	615
fr03	ChRM	7	yes	7.2	180.0	−40.3	181.9	−26.6	615	670
fr04	A	5	no	5.1	16.4	58.2	15.5	44.2	0	250
fr04	B	9	no	18.3	114.7	36.9	103.9	38.4	400	615
fr04	ChRM	6	yes	5.4	173.3	−33.5	175.5	−20.3	630	670
fr05	A	6	no	3.1	21.6	48.4	19.9	34.5	0	300
fr05	B	10	no	10.1	52.5	3.2	52.8	−7.6	450	645
fr05	ChRM	5	yes	14.2	174.0	−37.6	176.6	−24.2	645	670
fr06	A	5	no	5.6	2.2	70.4	6.6	56.7	0	250
fr06	ChRM	17	yes	5.5	171.6	−33.1	174.0	−20.0	300	670
fr07	A	6	no	1.8	357.7	73.4	4.4	59.6	0	300
fr07	ChRM	17	yes	7.2	186.8	−50.1	188.1	−36.2	300	670
fr08	A	6	no	8.4	17.4	43.5	16.7	29.6	0	300
fr08	ChRM	17	yes	6.6	201.6	−46.4	200.0	−32.6	300	670
fr09	A	5	no	2.9	47.8	41.7	42.4	29.6	0	250
fr09	ChRM	18	yes	6.0	188.6	−43.1	189.3	−29.1	250	670
frl0	A	5	no	6.1	38.6	52.1	33.0	39.3	0	250
frl0	ChRM	18	yes	3.8	178.0	−36.0	179.9	−22.4	250	670

Table A1. (*Continued.*)

Sample	Comp.	*N*	Anch.	MAD	GDECL	GINCL	BDECL	BINCL	Low T	High
frll	A	5	no	6.3	220.0	49.9	231.1	61.7	0	250
frll	ChRM	18	yes	2.6	98.9	−41.9	111.4	−41.4	250	670
frl2	A	4	no	10.5	10.8	58.1	11.3	44.4	0	200
frl2	ChRM	18	yes	3.4	185.3	−47.9	186.8	−34.0	250	670
frl3	A	5	no	5.3	6.6	55.4	8.1	41.5	0	250
frl3	ChRM	17	yes	6.8	180.8	−24.4	181.8	−10.7	300	670
frl4	A	5	no	6.8	1.1	52.8	3.8	39.1	0	250
frl4	ChRM	17	yes	4.0	198.2	−34.9	197.6	−20.9	300	670
frl5	A	5	no	2.0	8.4	64.2	9.8	50.2	0	250
frl5	ChRM	18	yes	3.2	191.2	−37.4	191.5	−23.4	250	670
frl6	A	5	no	8.5	0.5	38.6	2.3	24.9	0	250
frl6	ChRM	18	yes	3.1	206.6	−47.8	204.0	−34.1	250	670
frl7	A	5	no	7.6	5.2	43.1	6.6	29.2	0	250
frl7	B	11	no	19.3	70.8	41.8	62.0	33.4	300	615
frl7	ChRM	7	yes	15.3	183.6	−28.3	184.5	−14.5	615	670
frl8	A	5	no	4.2	15.7	62.4	15.0	48.4	0	250
frl8	ChRM	12	yes	5.4	172.3	−32.6	174.6	−19.4	500	670
frl9	A	5	no	3.8	38.3	61.0	31.0	48.0	0	250
frl9	ChRM	17	yes	9.2	179.0	−30.2	180.4	−16.6	300	670
fr20	A	5	no	4.1	341.3	46.5	347.1	34.2	100	300
fr20	B	9	no	12.2	304.7	24.6	309.8	18.7	350	600
fr20	ChRM	8	yes	10.9	200.7	−31.1	199.9	−17.1	600	670
fr21	A	6	no	3.6	357.5	52.7	1.0	39.1	0	300
fr21	B	11	no	4.5	333.9	55.8	343.4	44.2	350	630
fr21	ChRM	6	yes	16.2	202.0	−26.6	201.3	−12.8	630	670
fr22	A	6	no	5.2	29.9	36.0	27.7	22.6	0	300
fr22	B	7	no	24.1	30.2	−0.6	30.8	−13.9	350	550
fr22	ChRM	10	yes	8.5	188.2	−44.0	189.0	−30.0	550	670
fr23	A	6	no	2.4	6.9	46.2	7.9	32.3	0	300
fr23	B	10	no	5.8	6.8	28.1	7.3	14.2	300	600
fr23	ChRM	7	yes	8.9	197.8	−49.7	196.8	−35.8	600	670
fr24	A	5	no	3.8	353.7	64.2	359.9	50.7	0	250
fr24	B	6	no	18.0	107.9	76.5	59.9	71.5	400	550
fr24	ChRM	10	yes	6.3	188.5	−28.1	188.9	−14.2	550	670
fr25	A	6	no	4.0	349.6	58.2	355.8	45.1	0	300
fr25	B	8	no	12.1	330.9	88.8	10.0	75.1	300	550
fr25	ChRM	6	yes	5.0	191.9	−15.1	192.0	−1.1	615	670
fr26	A	5	no	1.7	351.3	48.8	355.6	35.6	100	300
fr26	B	13	no	4.8	357.5	55.7	1.3	42.1	300	645
fr26	ChRM	5	yes	5.5	181.2	−20.4	181.9	−6.6	645	670
fr27	A	6	no	2.9	6.2	54.3	7.8	40.4	0	300
fr27	B	11	no	4.1	26.2	60.8	22.4	47.1	350	630
fr27	ChRM	6	yes	8.4	192.6	−35.9	192.7	−21.9	630	670
fr28	A	5	no	2.6	40.9	64.6	31.9	51.7	0	250
fr28	B	9	no	8.9	70.5	53.4	57.9	44.6	300	575
fr28	ChRM	9	yes	14.6	216.1	−45.0	212.1	−31.9	575	670
fr29	A	6	no	3.8	358.2	57.3	2.0	43.6	0	300
fr29	B	10	no	12.5	5.6	46.4	7.0	32.5	350	615
fr29	ChRM	7	yes	12.4	204.4	−53.9	201.8	−40.1	615	670
fr30	A	7	no	3.9	45.2	48.5	39.0	36.2	0	350
fr30	B	10	no	10.6	21.8	35.5	20.7	21.7	450	645
fr30	ChRM	5	yes	16.2	198.9	−54.5	197.5	−40.5	645	670
cc01	A	3	no	3.3	253.1	62.2	288.8	28.7	0	150
cc01	B?	7	no	6.4	296.2	32.1	299.3	−10.4	150	450
cc02	A	5	no	10.3	359.5	54.8	341.1	16.0	0	250
cc02	ChRM	14	yes	2.0	190.9	−26.8	183.3	3.3	300	670
cc03	A	4	no	9.0	128.2	−40.1	130.7	4.6	100	250
cc03	ChRM	14	yes	1.9	172.3	−40.7	163.1	−1.2	300	670
cc04	A	3	no	8.3	286.1	61.3	302.0	19.2	100	200
cc04	ChRM	15	yes	4.1	208.6	−31.2	192.7	−9.8	250	670
cc05	A	4	no	11.7	67.2	67.2	350.6	48.1	0	200
cc05	ChRM	14	yes	1.8	186.5	−34.0	176.2	−0.7	300	670
cc06	A	4	no	14.4	126.4	72.2	324.7	62.3	0	200
cc06	ChRM	15	yes	2.0	186.0	−25.5	180.4	6.7	250	670

Table A1. (*Continued.*)

Sample	Comp.	*N*	Anch.	MAD	GDECL	GINCL	BDECL	BINCL	Low T	High
cc07	A	5	no	6.5	202.9	38.2	243.6	42.0	0	250
cc07	ChRM	13	yes	2.3	191.6	−21.9	186.7	6.9	300	655
cc08	A	6	no	5.6	167.9	−23.5	166.4	16.1	0	300
cc08	ChRM	13	yes	1.2	174.6	−41.9	164.2	−3.1	300	655
cc09	A	5	no	12.7	39.2	65.4	348.5	36.9	0	250
cc09	ChRM	15	yes	3.1	212.2	−40.2	188.3	−18.4	250	670
cc10	A	4	no	8.0	136.7	60.9	318.8	74.1	0	200
cc10	ChRM	15	yes	4.1	212.0	−36.3	191.1	−15.5	250	670
cc11	A	4	no	8.0	185.6	26.9	219.0	47.8	0	200
cc11	ChRM	15	yes	1.9	200.7	−40.3	181.6	−12.4	250	670
cc12	A	4	no	5.1	243.9	34.4	262.9	13.6	0	200
cc12	ChRM	15	yes	3.1	196.1	−40.6	178.7	−10.4	250	670
cc13	A	4	no	14.4	198.7	58.8	270.8	51.1	100	250
cc13	ChRM	15	yes	3.5	209.9	−30.3	194.2	−9.9	250	670
cc14	A	3	no	12.5	203.0	44.7	251.5	44.9	100	200
cc14	ChRM	15	yes	2.3	206.3	−35.4	188.3	−11.7	250	670
cc15	A	4	no	5.6	198.1	58.1	269.6	51.5	0	200
cc15	ChRM	13	no	6.1	219.7	−21.7	206.6	−10.0	250	640
cc16	A	5	no	11.0	125.5	−27.1	126.4	17.1	0	250
cc16	ChRM	11	no	8.7	197.0	−47.7	174.6	−16.4	400	655
cc17	A	4	no	2.3	340.9	82.7	321.1	38.3	0	200
cc17	ChRM	14	no	12.6	227.5	−56.0	181.1	−35.9	250	655
cc18	A	4	no	4.3	1.7	71.1	332.7	30.4	0	200
cc18	ChRM	15	yes	5.3	196.7	−50.5	172.6	−18.4	250	670
cc19	A	3	no	6.7	237.6	31.4	256.8	15.0	100	200
cc19	ChRM	11	no	9.9	232.5	−30.8	207.6	−24.6	250	600

From left to right: Sample (fr, Forada; cc, Cicogna); Comp., magnetic component (see text); *N*, number of demagnetization steps used to define the component; Anch.: yes (no), component (not) anchored to the origin of the demagnetization axes; MAD, maximum angular deviation (°); GDEC, GINC, BDEC, BINC, declination and inclination of the component in geographic and tilt corrected coordinates (°), respectively; Low T and High T, lower and higher unblocking temperature (°C) of the component.